Journal of Geochemical Exploration 154 (2015) 180–193

Contents lists available at ScienceDirect

Journal of Geochemical Exploration

journal homepage: www.elsevier.com/locate/jgeoexp

Analysis and mapping of soil geochemical anomalies: Implications for bedrock mapping and gold exploration in Giyani area, South Africa

Martiya Sadeghi [a,*], Alazar Billay [b], Emmanuel John M. Carranza [c]

[a] Geological Survey of Sweden, Uppsala, Sweden
[b] Council for Geoscience, Pretoria, South Africa
[c] James Cook University, Townsville, Australia

ARTICLE INFO

Article history:
Received 3 June 2014
Revised 15 November 2014
Accepted 19 November 2014
Available online 13 December 2014

Keywords:
Soil geochemistry
Gold mineralisation
Compositional data
PCA
Giyani South Africa

ABSTRACT

Previous exploration activities in the Giyani greenstone belt (GGB) were guided by the availability of outcrops, particularly iron formation, as this rock was considered to be the main host rock for gold mineralisation in the belt, although the majority of the known prospects/deposits are hosted by mafic rocks. However, there is no reliable lithological map available for the GGB, because most of it is covered by regolith, and thus in the early 1990s most mining and exploration companies in the GGB have abandoned their work as they were discouraged by the scarcity of outcrops, the small sizes of existing deposits and the low gold prices at that time. In the present study, major and trace element geochemical data from a high-density soil geochemical survey (1 sample/km^2) have been subjected to statistical and spatial analyses to support bedrock mapping and gold exploration. Maps are presented for major oxides, trace elements and selected respective ratio maps, and principal components (PC). The PC analysis was performed on clr-transformed data of selected trace elements known to be associated with gold mineralisation. The first six PCs explain about 78% of the total variance. PC4 representing Sb–As–Te–Cr–Au association best reflects the known gold mineralisation and was, therefore, used as a thematic layer. The information provided by various composite maps of different major/trace element data, as well as PC maps, has been used to produce an interpretive bedrock map outlining major lithological units in the study area. As gold mineralisation in the Giyani greenstone belt is hosted by certain known lithologies, the map is useful in indicating potential gold bearing areas.

1. Introduction

Various state geological surveys, including the Council for Geosciences (CGS) of South Africa, have been investigating ways for effective analysis and interpretation of soil geochemistry data for mineral exploration and bedrock mapping purposes. Methods of multivariate data analysis, such as principal component (PC) and factor analysis, are widely used for the statistical processing of exploration geochemical data (e.g., Carranza, 2010; El-Makky, 2011; Sadeghi et al., 2013a; Zuo, 2011). These methods commonly aim to reduce the dimensionality of variables or to identify a few but relevant factors depicting processes that explain a large proportion of variance in a multivariate data set (Davis, 1973, 1986, 2002; Reimann et al., 2008).

During the last few decades, several publications address the effect of outliers and anomalies on compositional data processing (e.g., Carranza, 2011; Grunsky et al., 2014; Pawlowsky-Glahn and Buccianti, 2011; Reimann et al., 2008, 2012). Outliers in geochemical data should always be examined carefully to ascertain that they are not the result of analytical or sampling error (Grunsky, 2010; Reimann et al., 2008; Thompson, 1983). In practice, outliers are usually assessed by graphical examination of upper and lower rankings of data, and the identification of values that occur as distinct breaks from the background population (Grunsky, 2010; Lepeltier, 1969; Sinclair, 1976, 1983, 1986, 1991; Tennant and White, 1959).

Geochemical data are typically reported as parts of a total composition (ppm, weight %, etc.) and, thus, geochemical data analyses are affected by the closure problem (Grunsky et al., 2014; Reimann et al., 2008, 2012). Accordingly, since geochemical data are compositional, every data set should be opened, prior to its statistical treatment, using a preferred method from a variety of suggested methods (Carranza, 2011; Reimann et al., 2008). There are three different log-ratio transformation methods for opening of compositional data, namely (1) additive log-ratio or alr (Aitchison, 1986), (2) centred log-ratio or clr (Aitchison, 1986), and (3) isometric log-ratio or ilr (Egozcue et al., 2003). There is much debate as to which method gives the best result for mapping spatial distribution of pathfinder elements in mineral exploration. Carranza (2011) has shown that either clr- or ilr-transformed stream sediment geochemical data are superior to alr-transformed stream sediment geochemical data for recognising anomalous multi-element signatures associated with mineralisation. This is

* Corresponding author at: Geological Survey of Sweden, Villavägen 18, PO Box 670, SE 751 28 Uppsala, Sweden. Tel.: +46 18 179232; fax: +46 18 179210.
E-mail address: martiya.sadeghi@sgu.se (M. Sadeghi).

http://dx.doi.org/10.1016/j.gexplo.2014.11.018
0375-6742/

due to the fact that ilr is an isometric transformation and the direct relation to the elements is lost, while in the clr-transformation each variable is divided by the geometric mean of all elements measured, followed by log-transformation and, therefore, preserves the so-called Aitchison distance in the sample space of compositional data. The alr-transformation is not isometric, because it uses one variable for the ratio, and different results can be expected when a different variable (elements/oxide) is used as denominator (Aitchison, 1986; Egozcue et al., 2003).

Since 1973, the CGS has been conducting regional (1 sample/km^2) soil geochemical surveys for mineral exploration so as to recognise new prospective areas in geologically favourable terranes (Lombard et al., 1999). One such geologically permissive terrane is the Archaean Giyani Greenstone Belt (GGB) in the Limpopo Province, South Africa, which is known for its gold mineralisation. In the GGB, there are at least 40 currently known gold occurrences (Ward and Wilson, 1998), which are hosted mainly in mafic metavolcanic rocks and iron-formations (Billay et al., 2009). Due to the scarcity of outcrops in the GGB, there is a lack of an accurate bedrock map to support recognition of new prospective areas. Therefore, the aim of this paper is to demonstrate and to highlight the benefits of soil geochemical data processing and interpretation for bedrock mapping and gold exploration in the GGB.

2. Study area

At their present level of exposure, the Archaean rocks of the Kaapvaal Craton are dominated by 3.64 Ga granitoid gneiss (Armstrong et al., 1990) and various 2.65 Ga granitoid masses (Barton and Van Reenen, 1990). Within this granite–gneiss terrane, belts of metavolcanic rocks occur, of which the Barberton, Murchison, Pietersburg and Giyani greenstone belts are spatially the most dominant (McCourt and Van Reenen, 1992).

The NE-trending GGB is situated at the north-eastern edge of the Kaapvaal Craton in the Limpopo province of South Africa (Fig. 1). It is ~15 km wide and ~70 km long and bifurcates towards its south-western end into the northern Khavagari branch and the southern Lwaji branch. The supra-crustal rocks in the GGB (Giyani Group; SACS, 1980) are flanked to the north by migmatised tonalitic gneiss (Klein Letaba Gneiss) and to the south by younger granite. Within the GGB, geophysical modelling by Kleywegt et al. (1987) indicates the thickness of the Giyani Group to be between 1.5 and 3 km, increasing towards the SE margin of the belt. They also concluded that the GGB is not situated along a major crustal boundary. The GGB is predominantly made up of ultramafic–mafic rocks with minor intercalations of various types of iron-formation, felsic schist and pelitic metasediments (Brandl et al., 2006; McCourt and Van Reenen, 1992; Prinsloo, 1977).

The GGB has been subjected to complex polyphase deformation. The most comprehensive structural studies on the GGB can be found in McCourt and Van Reenen (1992) and De Wit et al. (1992). In summary, McCourt and Van Reenen (1992) describe three ductile-deformation phases comprising (i) an older penetrative deformation (D_1), (ii) a younger non-penetrative deformation (D_2) and (iii) the latest deformation event (D_3) characterised by discrete strike–slip shear zones. The D_1 phase gave rise to N-trending regional schistocity and was responsible for ENE–WSW and E–W-trending, north-dipping oblique to reverse shear zones, as well as the associated reclined sheath folds and a well-developed mineral lineation. The non-penetrative D_2 phase was superimposed on D_1 structures, and can be recognised by either eastward plunging folds of the regional foliation or related horizontal

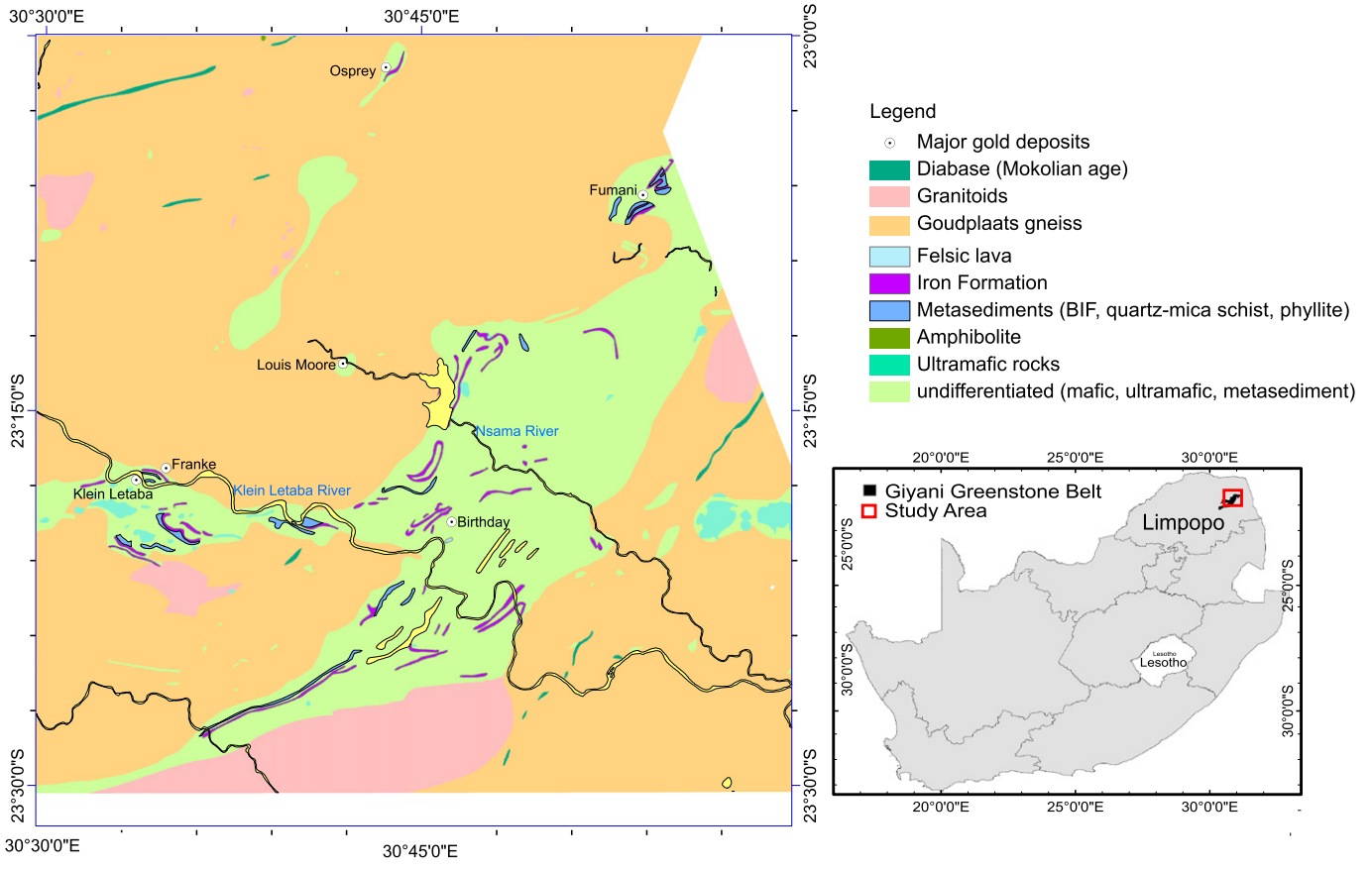

Fig. 1. Location (inset) and general geology of the Giyani greenstone belt and the surrounding granite–greenstone terrane.

crinkle lineations. The D_3 phase is associated with the development of discrete strike–slip shear zones at the margins of the GGB post-dating granitoid intrusion. McCourt and Van Reenen (1992) suggest that the steeply dipping left-lateral brittle–ductile shear zones (D_3) and ultramylonite along the tectonic boundary of the high-grade retrograde granulite (to the north), and the lower grade rocks of the GGB, are a part of the progressive D_2 deformation (late-D_2).

3. Soil geochemical data

3.1. Soil geochemical sampling

A high-density programme of regional geochemical soil sampling has been undertaken by the CGS since 1973 (Lombard et al., 1999). A total of 2725 soil samples, about 5 kg per sample, were collected from the top 25 cm of the soil at a sampling density of 1 sample/km^2. Details of the sampling, sample preparation and quality control procedure are described in Maritz et al. (2010). Maritz et al. (2010) showed that there is an excellent correlation between soil chemical composition and underlying lithological formations in the Giyani area, and they suggested certain elements for discriminating granitoid masses in the Giyani area.

The <75 μm soil fraction was analysed by: (i) XRF for 10 major/minor oxides, namely SiO_2 (33), TiO_2 (7.4), Al_2O_3 (30), Fe_2O_3 (6.5), MnO (4.8), MgO (10), CaO (4.3), Na_2O (7.7), K_2O (6.3) and P_2O_5 (5.7), and for 28 elements, namely Ag (1.7), As (1.5), Ba (8.8), Ce (12), Co (3.6), Cr (4.4), Cu (0.5), Ga (0.4), Hf (0.5), Mo (0.4), Nb (3.8), Nd (1.7), Ni (0.6), Pb (3.9), Rb (0.3), S (2), Sb (0.8), Sc (6.6), Sn (1.3), Sr (0.3), Ta (0.5), Th (2), U (2), V (4.7), W (1.9), Y (0.4), Zn (0.3) and Zr (2.6) at the CGS laboratory in Pretoria, South Africa (Maritz et al., 2010); the number in parentheses is the lower detection limit (DL) in ppm of each element/oxide; (ii) DC arc emission spectrography for Au (0.0005), Pt (0.009) and Pd (0.009) at the Henan Laboratory, Peoples Republic of China; and (iii) ICP-MS for 46 elements after HF–HClO4 digestion (Li (2.9), Be (0.06), Mg (0.008), P (0.002), Ca (0.02), Sc (0.28), Ti (0.0004), V (0.73), Cr (30.58), Mn (0.0003), Fe (0.02), Co (0.16), Cu (21.73), Zn (19.98), Ga (0.18), Rb (0.06), Sr (0.81), Y (0.02), Zr (0.54), Mo (0.41), Ag (0.45), Cd (0.03), Sb (0.03), Te (0.02), Cs (0.07), Ba (8.65), La (0.09), Ce (0.10), Pr (0.01), Nd (0.05), Sm (0.01), Eu (0.01), Gd (0.01), Tb (0.07), Dy (0.01), Ho (0.01), Er (0.01), Tm (0.01), Yb (0.01), Lu (0.01), Ta (0.01), Tl (0.01), Pb (0.51), Bi (0.04), Th (0.01), U (0.01)). All the mentioned analytical methods are certified and quality-controlled using duplicate, replicate and standard samples, details of which have been described by Maritz et al. (2010). The average relative standard deviation (RSD) for the duplicate XRF analyses varied from 0.5% to 4%, whereas the ICP-MS duplicate analyses had a RSD of 7%. In this study, the major oxide data from XRF analysis were used, and trace elements data from ICP-MS analysis. The latter geo-analytical method was employed because of its low DL, which is useful for the determination of trace elements (e.g., Te and Bi) that are generally known to be associated with orogenic-gold deposits. The basic statistics of the major/minor oxide and trace element data are given in Table 1.

Table 1
Summary statistics of major oxides and trace elements. Analysis of oxides by XRF and trace elements by ICP-MS after HF–ClO_4 extraction. MAD: median absolute deviation. All values are in ppm.

Elements	Minimum	Median	MAD	Maximum
SiO_2	247,456	527,004	32,449	705,667
TiO_2	3153	14,897	2810	41,326
Al_2O_3	33,158	142,176	12,679	207,179
Fe_2O_3	12,292	77,193	24,072	226,189
MnO	1501	11,875	3272	68,911
MgO	<10	9205	4307	222,492
CaO	5707	16,689	3512	245,565
Na_2O	<7.7	12,202	3898	36,806
K_2O	814	15,112	5106	46,200
P_2O_5	322	989	184	22,938
Li	3.83	19.6	6.47	205
Be	0.11	2.09	0.45	16.6
Sc	2.51	15.3	5.78	49.5
V	25.4	137	48.2	869
Cr	30.6	215	112	13,999
Mn	144	1222	347	6700
Fe	6905	54,886	18,901	259,223
Co	3.14	27.3	11.0	250
Cu	21.7	70.0	25.2	404
Zn	20.0	89.3	20.9	814
Ga	6.08	23.6	3.17	45.0
Rb	5.34	76.6	20.9	440
Sr	12.3	312	113	1323
Y	2.75	15.7	4.19	52.2
Zr	4.19	108	23.0	554
Mo	0.41	0.59	0.18	4.03
Cd	0.03	0.05	0.02	0.53
Sb	0.03	0.23	0.09	19.9
Te	0.02	0.02	0.00	0.23
Cs	0.38	3.55	1.32	131
Ba	35.8	651	216	15,142
Ta	0.04	1.02	0.24	15.7
Tl	0.04	0.45	0.14	2.09
Pb	1.71	19.83	6.32	1574
Bi	0.04	0.14	0.06	7.24
Th	0.53	6.34	2.20	110
U	0.08	0.98	0.34	7.83
As	<1.5	0.006	0.006	0.254
Pt	0.0005	0.002	0.001	0.212
Au	0.009	0.002	0.001	0.173
Pd	0.009	0.002	0.001	0.030

3.2. Dealing with censored geochemical data

A primary purpose of geochemical data analysis is to identify geochemical/geological processes based on statistical and spatial variations in a data set (e.g., Aitchison, 1986; Bonham-Carter et al., 1988, 1989; Carranza, 2010; Cheng et al., 2000; El-Makky, 2011; El-Makky and Sediek, 2012; Grunsky et al., 2014; Luz et al., 2014; Singer and Kouda, 2001). Variations in geochemical data are, however, commonly influenced by censored values (i.e., values below analytical DL). Such values are commonly replaced by a value equal to ½ the DL. This practice usually yields suitable results when there are only few censored values.

In this study, censored values were first examined. Censored values of Pd (4 samples), Au (4 samples), Pt (4 samples), and As (685 samples) are replaced by values equal to ½ of their respective DLs as it is a customary procedure in geochemistry. Secondly, because of high percentages of censored values of As (about 40% of total samples), PC analysis was run two times; the first with As data (including censored values replaced by ½ the value of DL, hereafter referred to as **As^r**), and the second without As data. In a previous study of the effect of censored data on mapping multi-element anomalies, Carranza (2011) demonstrated that exclusion of As data, with about 30% of the samples having censored values, barely improved mapping of multi-element anomalies as compared to inclusion of As data with **As^r**. In this study, the effect of including or excluding censored values (ca. 40% of As samples) in PC analysis of element associations and on mapping of multi-element geochemical anomalies was evaluated.

3.3. Multivariate geochemical data analysis

Among the various multivariate statistical methods for revealing patterns attributed to geological and mineralisation processes (Grunsky, 2010), PC analysis has been used for studying geochemical data structures (see Sadeghi et al., 2013a and references therein). The foundation of PC analysis is the correlation (covariance) matrix, which describes the relationships between variables. For mapping of anomalies representing a multi-element signature of mineralisation, log-ratio transformed data sets should be used in PC analysis (Carranza, 2011).

Table 2
Principal components of ln- and clr-transformed data including As, and clr-transformed data with As excluded.

Element	PCs of ln-transformed data including censored As						Element	PCs of clr-transformed data including censored As						Element	PCs of clr-transformed data excluding As					
	PC1	PC2	PC3	PC4	PC5	PC6		PC1	PC2	PC3	PC4	PC5	PC6		PC1	PC2	PC3	PC4	PC5	PC6
Li	−0.26	**0.67**	**−0.52**	−0.12	−0.03	0.10	Li	−0.29	**−0.64**	**0.53**	−0.14	−0.02	0.1	Li	0.1	**0.75**	**−0.37**	0.01	0	0.2
Be	0.39	**0.76**	−0.15	−0.07	−0.02	−0.11	Be	0.35	**−0.78**	0.16	−0.08	−0.01	−0.11	Be	**0.82**	0.12	−0.2	−0.04	0.14	0.09
Sc	**−0.89**	0.31	0.12	−0.11	−0.01	0.03	Sc	**−0.92**	−0.26	−0.1	−0.1	−0.01	0.03	Sc	**−0.9**	−0.05	−0.28	0.05	0.07	0.05
V	−0.37	−0.05	0.06	0.06	−0.27	0.00	V	**−0.87**	−0.28	−0.27	−0.06	−0.07	−0.01	V	**−0.83**	−0.27	−0.29	−0.02	0.08	−0.06
Cr	**−0.76**	0.01	−0.14	0.33	0.04	−0.08	Cr	**−0.75**	0.04	0.16	**0.34**	0.01	−0.07	Cr	**−0.7**	0.22	**0.35**	−0.21	−0.02	−0.27
Mn	**−0.81**	0.34	0.22	0.09	−0.18	0.02	Mn	**−0.83**	−0.29	−0.19	0.09	−0.18	0.03	Mn	**−0.75**	−0.24	−0.17	−0.3	−0.05	−0.18
Fe	**−0.88**	0.30	0.23	−0.02	−0.09	−0.03	Fe	**−0.91**	−0.26	−0.21	−0.01	−0.1	−0.02	Fe	**−0.89**	−0.23	−0.23	−0.13	0.08	−0.06
Co	**−0.91**	0.20	0.07	0.08	−0.04	−0.06	Co	**−0.92**	−0.14	−0.04	0.09	−0.06	−0.05	Co	**−0.9**	0.01	−0.02	−0.16	0.06	−0.17
Cu	**−0.78**	0.40	0.26	−0.16	0.03	0.02	Cu	**−0.81**	−0.36	−0.25	−0.15	0.04	0.02	Cu	**−0.73**	−0.24	**−0.39**	0.16	0.13	0.12
Zn	**−0.61**	0.43	0.35	0.06	−0.30	−0.05	Zn	**−0.64**	−0.4	−0.33	0.07	−0.31	−0.02	Zn	−0.41	−0.44	−0.26	**−0.46**	−0.06	0.03
Ga	0.28	**0.75**	0.30	−0.19	−0.03	−0.13	Ga	0.22	**−0.77**	−0.3	−0.19	−0.02	−0.14	Ga	**0.7**	−0.4	−0.19	−0.03	0.18	0.26
Rb	**0.58**	**0.68**	−0.17	−0.01	0.10	0.10	Rb	**0.54**	**−0.71**	0.17	−0.02	0.12	0.09	Rb	**0.89**	0.12	−0.13	0.08	−0.01	0.06
Sr	**0.65**	0.13	**0.48**	0.11	−0.08	−0.26	Sr	**0.63**	−0.18	**−0.49**	0.12	−0.09	−0.25	Sr	**0.68**	**−0.51**	0.16	−0.13	0.05	0
Y	−0.50	**0.63**	0.24	−0.27	−0.02	0.19	Y	−0.54	**−0.61**	−0.22	−0.25	0	0.19	Y	−0.24	−0.25	**−0.71**	0.2	0	0.19
Zr	0.39	**0.58**	**0.47**	0.05	−0.07	0.23	Zr	0.34	**−0.61**	−0.46	0.06	−0.04	0.24	Zr	**0.67**	−0.46	−0.16	0.03	−0.18	−0.19
Mo	−0.37	0.46	0.09	0.20	0.26	**−0.45**	Mo	−0.39	−0.44	−0.06	0.21	0.21	**−0.48**	Mo	−0.06	−0.07	0.21	−0.06	**0.77**	−0.18
Cd	−0.53	0.28	−0.05	0.24	−0.29	−0.01	Cd	**−0.54**	−0.24	0.08	0.24	−0.32	0.03	Cd	−0.3	0.03	0.08	**−0.53**	−0.26	**0.51**
Sb	−0.45	0.15	−0.18	**0.55**	−0.11	**0.36**	Sb	**−0.45**	−0.12	0.2	**0.54**	−0.11	0.35	Sb	−0.31	0.24	**0.31**	−0.17	**−0.47**	−0.04
Te	−0.47	0.17	−0.01	**0.40**	0.21	−0.27	Te	**−0.47**	−0.14	0.04	**0.41**	0.18	−0.27	Te	−0.16	−0.12	**0.44**	−0.22	0.27	**0.47**
Cs	−0.14	**0.69**	**−0.59**	−0.05	−0.01	−0.04	Cs	−0.16	**−0.67**	**0.61**	−0.06	−0.01	−0.04	Cs	0.23	**0.82**	−0.27	−0.04	0.12	0.02
Ba	**0.70**	0.30	0.43	0.18	0.13	−0.20	Ba	**0.67**	−0.35	−0.44	0.19	0.11	−0.21	Ba	**0.78**	**−0.45**	0.19	−0.01	0.09	−0.07
Ta	0.13	**0.72**	0.01	−0.05	**−0.30**	0.11	Ta	0.09	**−0.73**	0	−0.06	−0.27	0.13	Ta	0.51	0.08	**−0.41**	−0.14	−0.19	−0.32
Tl	**0.63**	0.66	−0.20	0.02	0.10	0.01	Tl	0.59	**−0.69**	0.2	0.01	0.11	0	Tl	**0.91**	0.15	−0.08	0.03	0.03	0.05
Pb	**0.73**	0.42	0.19	0.20	0.14	−0.12	Pb	**0.7**	**−0.47**	−0.19	0.21	0.12	−0.13	Pb	**0.86**	−0.25	0.16	−0.03	0.07	−0.01
Bi	−0.16	0.56	**−0.55**	0.11	−0.02	−0.30	Bi	−0.18	−0.53	**0.56**	0.1	−0.05	−0.3	Bi	0.14	**0.72**	−0.03	−0.21	0.28	−0.1
Th	**0.61**	0.49	0.10	0.08	0.20	0.27	Th	**0.58**	**−0.52**	−0.1	0.1	0.21	0.27	Th	**0.81**	−0.14	0.01	0.12	−0.14	−0.02
U	**0.60**	**0.62**	−0.02	0.07	0.12	0.22	U	**0.57**	**−0.65**	0.02	0.08	0.13	0.23	U	**0.87**	0	−0.07	0.08	−0.14	−0.05
As	0.58	−0.13	0.09	**0.52**	−0.09	**0.25**	As	**0.59**	0.09	−0.1	**0.51**	−0.09	**0.25**	As	–	–	–	–	–	–
Pt	**−0.74**	0.06	0.12	−0.11	**0.41**	0.13	Pt	−0.73	−0.01	−0.1	−0.08	**0.46**	0.1	Pt	**−0.67**	−0.06	0.17	**0.49**	−0.03	0.09
Au	**−0.61**	0.01	0.06	0.27	**0.36**	0.19	Au	**−0.61**	0.03	−0.04	**0.28**	**0.38**	0.15	Au	**−0.54**	0.03	**0.38**	**0.32**	−0.16	0.05
Pd	**−0.75**	0.13	0.13	−0.14	**0.44**	0.15	Pd	**−0.75**	−0.08	−0.1	−0.11	**0.48**	0.11	Pd	**−0.69**	−0.02	0.09	**0.56**	−0.01	0.09
Eigenvalue	11.04	6.51	2.26	1.36	1.14	1.04	Eigenvalue	11.62	6.58	2.34	1.36	1.12	1.05	Eigenvalue	13.15	3.36	2.22	1.59	1.29	1
% of variance explained	35.63	21.01	7.3	4.37	3.66	3.37	% of variance explained	37.49	21.23	7.53	4.38	3.62	3.38	% of variance explained	43.82	11.21	7.39	5.29	4.3	3.34
Cum. % of variance	35.63	56.63	63.94	68.31	71.94	75.35	Cum. % of variance	37.49	58.72	66.26	70.64	74.26	77.64	Cum. % of variance	43.82	55.03	62.41	67.7	72	75.34

Significant values of PCs are indicated as bold.

Table 3
Explanation of the six principal components extracted from the ln − and clr-transformed trace element data, which explain 75% and 78% of total variance, respectively.

Component	(a) ln-transformed data			(b) clr-transformed data		
	% of variance explained	Association	Interpretation	% of variance explained	Association	Interpretation
PC1	35.6	(i) Sc–Cr–Mn–Fe–Co–Cu–Mo–Au–Pt–pd (ii) Rb–Sr–Ba–Tl	(i) Mafic–ultramafic rocks with high Au content; (ii) Granitoid masses	37.5	(i) Rb–Sr–Ba–Pb (ii) Sc–V–Cr–Mn–Fe–Co–Cu–Zn	(i) Presence of granitoid masses; (ii) Depicts occurrence of underlying mafic–ultramafic rocks (Fig. 4a)
PC2	21	Li–Be–Ga–Rb–Y–Cs–Ta–U	Reflects effects of metal-bearing fluids related to the crystallisation of granitoid rocks	21.2	Li–Be–Ga–Rb–Y–Zr–Cs–Ta–Th–U	Reflects granitoid rocks underlying the study area (Fig. 4b)
PC3	7.3	(i) Li–Cs–Bi (ii) Ba–Sr	Reflect different types of granitoid rocks	7.5	(i) Li–Cs–Bi (ii) Sr–Zr	Contact zones between granitoid and greenstone rocks and different types of granitoids (Fig. 4c)
PC4	4.4	Cr–Sb–Te–As–Au	It likely represents enrichment of elements in soil due to weathering and concentration of heavy minerals, and reflects the presence of gold mineralisation	4.4	Sb–As–Te–Cr–Au	Reflects the presence of gold mineralisation (Fig. 5a and b)
PC5	3.7	(i) Cd–Ta–V (ii) Pt–Au–Pd	(i) Reflects parts of the greenstone belt (ii) Suggest an association of heavy minerals derived from rocks due to weathering	3.6	(i) Zn–Cd–Ta (ii) Pt–Au–Pd	(i) Indicates parts of the greenstone belt with an enrichment in these precious metals (ii) Suggest an association of heavy minerals derived from rocks due to weathering
PC6	3.4	(i) Te–Mo (ii) Sb–Au	(i) granitoids bearing Au? (ii) Suggest an enrichment of metals in soil derived from greenstone rocks	3.4	(i) Te–Mo (ii) Sb–Au	(i) granitoids bearing Au? (ii) Suggest an enrichment of metals in soil derived from greenstone rocks

The ln- and clr-transformed censored data of elements used in this study include censored values of As, Au and Pt replaced by ½ of their respective DLs, and also clr-transformed data excluding As from the analyses. Carranza (2011) has investigated questions related to exclusion or inclusion of censored values and comparing the log-transformation methods (alr, clr, ilr) with ln transformation in geochemical exploration. The outlier recognition plays an essential role in the interpretation of geochemical data, and several methods have been suggested by statisticians and geochemists in this context (Carranza, 2011; Filzmoser, 2005). In order to detect outliers in this study, the mono-element data were subjected to box-and-whiskers plots (Carranza, 2009; Kürzl, 1988; Tukey, 1977; and references therein) using *STATISTICA 12* software. Outliers (in the transformed data) were excluded from PC analysis, but the scores of the excluded outlier samples were calculated using the factor loading matrix. In this study, PC analysis was carried out separately for major oxides and trace elements, because the two data sets were generated by two different analytical techniques with different extraction levels (i.e., total extraction of major oxides by XRF versus near-total extraction of trace elements by ICP-MS after aqua regia attack of samples) and different analytical precisions.

4. Results

To assist the readers in following the interpretation of the soil geochemical data in relation to bedrock and anomaly mapping, the lithological boundaries of the bedrock map, produced from a combination of soil geochemical, Landsat TM and airborne radiometric data sets (Billay et al., 2014), are superimposed on all the PC, ratio and composite geochemical maps.

4.1. Trace element associations

As described in Section 3, about 40% of the soil samples yielded censored As values. In this regard, the trace element PC analysis was tested firstly by including As data (with **As^r**), and secondly by excluding As data.

It is known that ln- and clr-transformations behave differently, and that taking ln-transformation is equivalent to analysing the data in a product space (for details, see Pawlowsky-Glahn et al., 2013). In this study, the results of PC analysis, using the ln- and clr-transformed data sets, were compared as a practical implication of this approach. The generated results are given in Table 2, and the explanations of the extracted principal components in Table 3. Many previous studies show the benefit of either clr- or ilr-transformation, compared to other data transformations (e.g., ln-transformation), in enhancing anomalous multi-element association reflecting the presence of mineralisation (e.g., Carranza, 2011). The PC analysis, performed in this study, using clr-transformed data has successfully opened the data and revealed multi-element associations accounting for substantial proportion of the data variability and, consequently, it was not necessary to use ilr-transformation, as this requires back-transformation to clr-space for interpretation.

The results of PC analysis of ln-transformed data including As with **As^r**, and PC analysis of clr-transformed data, including As with **As^r** and excluding As data, are presented in Table 2. The first six PCs of clr-transformed data, including As data with **As^r** and excluding As data, explain about 78% and 75% of total variation, respectively. The PC analysis, including As with **As^r**, yielded slightly higher total variance in the first six PCs. The PC1 of both, including and excluding As data, show a similar trace element association, representing granitoid masses and mafic–ultramafic units in the GGB. The PC2 of the clr-transformed data, including As with **As^r**, show association of trace elements related to different types of granitoid masses, and the PC2 of the clr-transformed data excluding As represents different types of granitoid masses, some enriched in Li and Cs (leucogranite and biotite granite). The PC3 of either ln- or clr-transformed data reflects different types of granitoid masses, but the PC3 of the clr-transformed data, including As with **As^r**, shows an association of Te–Au–Cr–Sb that probably

represents gold mineralisation. The PC4 of the clr-transformed data, including As with **As^r**, shows an association of pathfinder elements (Sb–As–Te–(Cr–Au–Cd)) reflecting gold mineralisation in the ultramafic–mafic rocks, while the PC4 (Pd–Pt–Au association) of the clr-transformed data, including As with **As^r**, lacks the typical gold associated elements Sb and Te (Billay et al., 2014), and the greenstone reflecting elements (e.g., Cr, Co, Ni; Billay et al., 2009, 2014). In the clr-transformed data, including As with **As^r**, a Pd–Pt–Au association is captured by PC5.

The projections of trace elements on the bi-dimensional space (Fig. 3) show the approximate degrees of association among the variables in the data sets. The biplots of PC1 versus PC2 reveal that ln-transformed variables are largely limited to a half-circle, whereas clr-transformed variables occupy the full two-dimensional space.

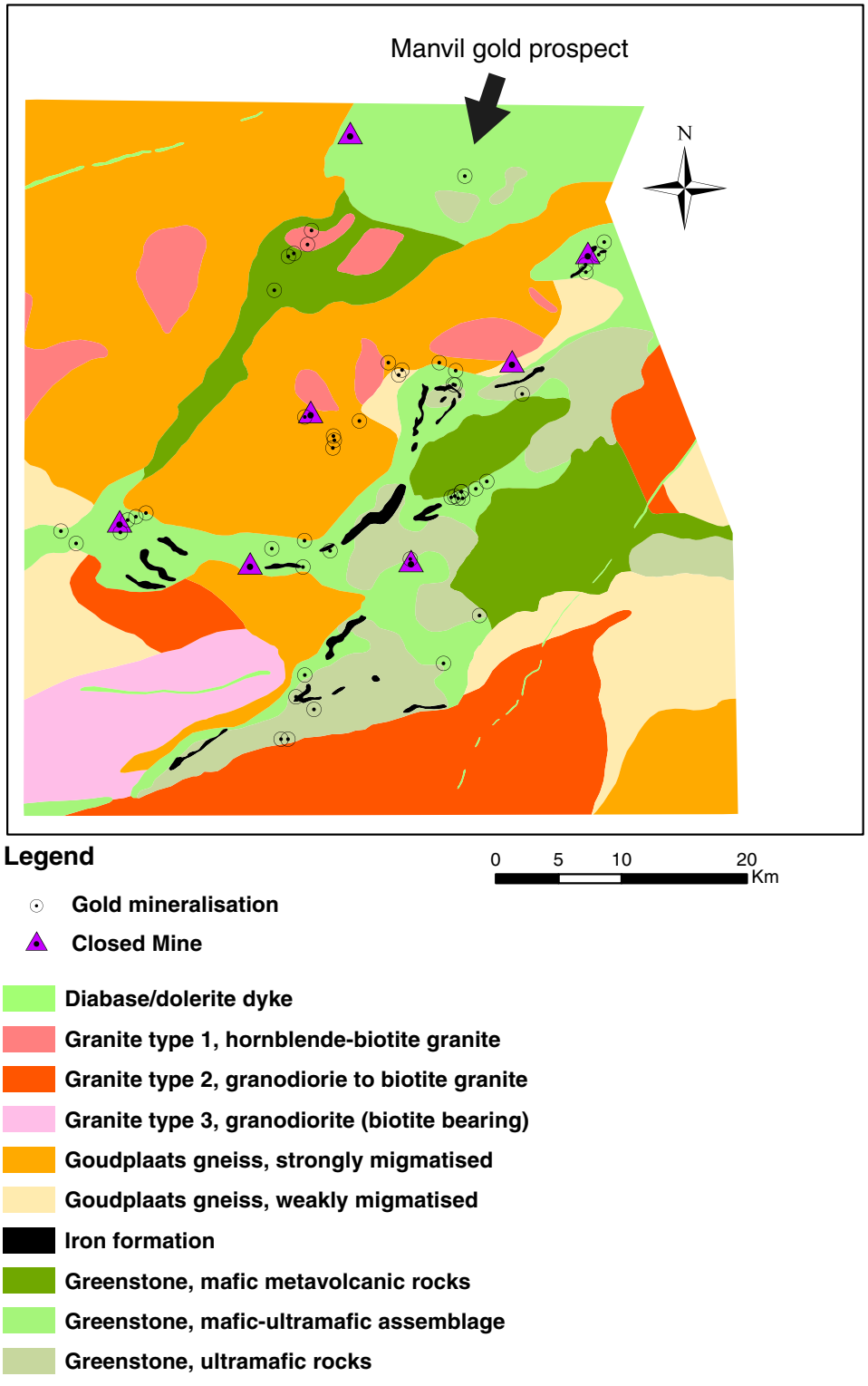

Fig. 2. Interpreted bedrock map in the GGB using soil geochemistry, airborne radiometric, DEM and Landsat TM data.

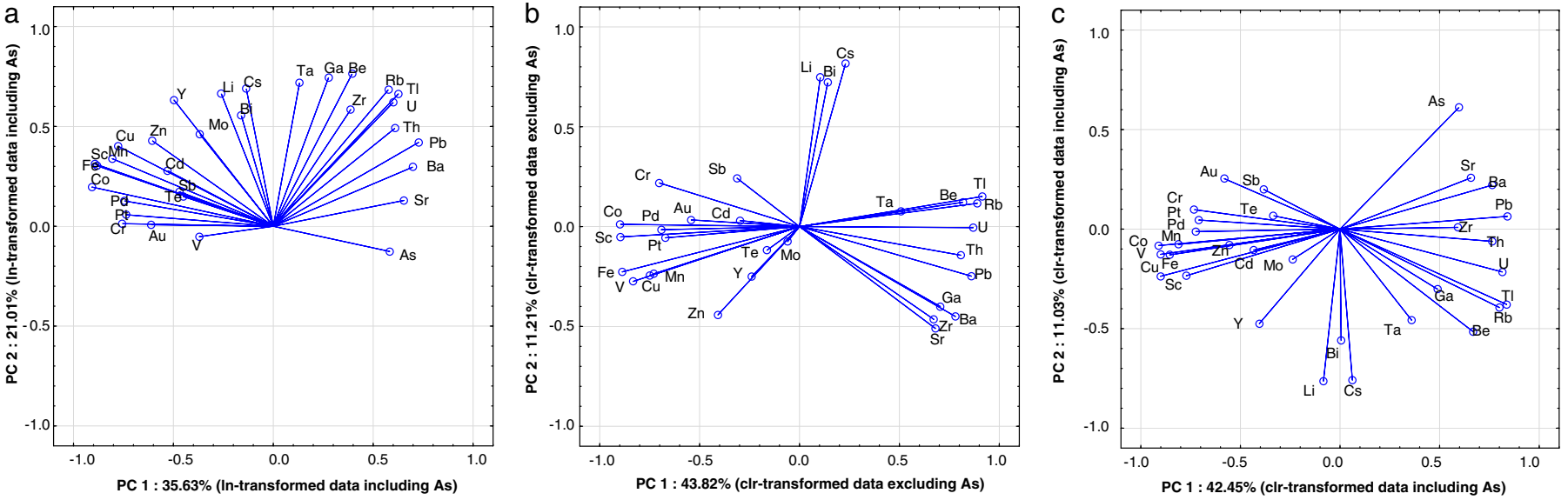

Fig. 3. Trace element biplots of PC1 vs. PC2 of (a) ln-transformed data including As with As^r (left panel); (b) clr-transformed data including As with As^r (middle panel), and (c) clr-transformed data excluding As data (right panel).

Table 4
Principal components of ln- and clr-transformed major oxide data.

Major oxide	ln-transformed data			Major oxide	clr-transformed data		
	PC1	PC2	PC3		PC1	PC2	PC3
SiO_2	**−0.70**	0.08	−0.28	SiO_2	**−0.69**	0.09	−0.12
TiO_2	0.13	**0.64**	**0.43**	TiO_2	0.12	**0.74**	**0.33**
Al_2O_3	−0.52	**0.43**	0.28	$Al2O_3$	−0.53	**0.42**	0.09
Fe_2O_3	**0.91**	0.30	0.06	Fe_2O_3	**0.89**	0.36	0.06
MnO	**0.83**	0.16	−0.06	MnO	**0.84**	0.24	0.12
MgO	**0.63**	−0.41	−0.48	MgO	**0.80**	−0.33	−0.13
CaO	0.33	**−0.69**	**0.36**	CaO	0.35	**−0.72**	0.19
Na_2O	**−0.83**	−0.21	0.04	Na_2O	**−0.80**	−0.18	0.23
K_2O	**−0.84**	−0.22	0.02	K_2O	**−0.84**	−0.11	0.28
P_2O_5	0.18	**−0.48**	**0.66**	P_2O_5	0.27	−0.17	**0.85**
Eigenvalue	4.22	1.67	1.14	Eigenvalue	4.45	1.61	1.06
% of variance explained	42.17	16.72	11.44	% of variance explained	44.53	16.13	10.61
Cum. % of variance	42.17	58.89	70.33	Cum. % of variance	44.53	60.66	71.27

Significant values of PCs are indicated as bold.

The latter data show three distinct element associations corresponding to mafic–ultramafic, older and younger granitoids, and appear to be more useful than the ln-transformed data in bedrock mapping and exploration.

To summarise the results for the ln- and clr-transformed data sets, the first six PCs of clr-transformed data explain about 78% of the total variance, while the first six PCs of ln-transformed data explain about 75% of total variance. Different PCs derived from ln- and clr-transformations are able to explain associations of PCs with the various underlying bedrock units, whereas the PC4 (association of Sb–As–Te–(Cr–Au–Cd)) of the clr-transformed data, including As with **As^r**, shows an association of pathfinder elements reflecting the presence of gold mineralisation in the GGB (Table 3).

The PC scores of the transformed data were gridded using the IDW interpolation method and a cell size of 1 ∗ 1 km. Although there are many interpolation methods, the IDW method has been chosen, because it is firstly a common deterministic point-to-surface interpolation technique, and secondly the soil sampling in the study area is of high density and systematic and, therefore, the data are strongly autocorrelated and can be sufficiently interpolated using this method (cf. Carranza, 2010).

4.2. Major oxides soil geochemical data

Results of PC analysis of the ln- and clr-transformed major element data are given in Table 4, and the explanations of the extracted PCs in Table 5.

The first two PCs of the ln- and clr-transformed major oxide data account for about 59% and 61% of total data variance, respectively. The projections of the 10 major elements on the bi-dimensional space (Fig. 6) show the degree of association among the variables in the data set, representing different lithologies, weathering and soil development processes. Fig. 6 depicts that clr-transformation is more efficient in discriminating various granitoids masses and mafic–ultramafic rock units in the study area.

4.3. Ternary and ratio maps using soil data

Ternary and element ratio maps of soil data have commonly been used in exploration geochemistry (e.g., Barnes, 1990; Beus and Grigorian, 1977; Brand, 1999; Chao and Theobald, 1976; Pawlowsky-Glahn and Buccianti, 2011; Reimann et al., 2014; Ziaii et al., 2011), and in the analysis of geophysical airborne radiometric data for interpretation of bedrock and mineralisation (e.g., De Quadros et al., 2003; Markandeyulu et al., 2013). An element ratio map or log-ratio map can assist in distinguishing mineralised from barren lithological bodies, in mapping lithology and in providing vectors towards ore environment (e.g., Beus and Grigorian, 1977; Garrett et al., 2008). Elemental ratio maps have also been used for environmental management purposes, risk assessments (e.g., Stanley and Noble, 2008); urban geology studies (e.g., Cicchella et al., 2008), and mapping of rare earth element distribution in soil (e.g., Sadeghi et al., 2013b).

In this study, log-ratio maps were plotted. In the log-ratio maps, negative values represent a dominance of the denominator, whereas positive values indicate dominance of the numerator, and zero indicates equality of both numerator and denominator. The plotted maps of element log-ratios are used to reflect contrasts in the chemical composition of the major lithologies in the study area. The log (Sr/Rb) ratio map (Fig. 7a) reflects compositional variation and/or the degree of metamorphism in the granitic rocks. Gneiss in the northern part

Table 5
Explanation of the three principal components extracted from the ln- and clr-transformed major oxide data, which explain 70% and 71% of total variance, respectively.

Component	(a) ln-transformed data			(b) clr-transformed data		
	% of variance explained	Association	Interpretation	% of variance explained	Association	Interpretation
PC1	42	(i) MgO–MnO–Fe_2O_3; (ii) SiO_2–Na_2O–K_2O	An antipathetic association depicting (i) ultramafic–mafic and (ii) granitic rocks	44	(i) Fe_2O_3–MnO–MgO; (ii) SiO_2–Al_2O_3–Na_2O–K_2O	An antipathetic association indicating (i) greenstone rocks, and (ii) certain types of granite
PC2	17	(i) TiO_2–Al_2O_3–(Fe_2O_3–MnO); (ii) CaO–P_2O_5;	An antipathetic association indicating amphibolite and weathering processes, and development of soil on (i) ultramafic and (ii) granitic rocks	16	(i) TiO_2–Al_2O_3–(Fe_2O_3); (ii) MgO–CaO	An antipathetic association depicting (i) the effects of metamorphism on the granitic gneiss and enrichment of immobile elements during weathering, and (ii) the ultramafic units within the GGB
PC3	11	TiO_2–CaO–P_2O_5	Reflects certain types of granitic–gneiss	11	(i) P_2O_5–TiO_2–(Na_2O–K_2O); (ii) SiO_2–MgO	An antipathetic association indicating (i) certain types of granitic–gneiss, and (ii) amphibolite within the GGB

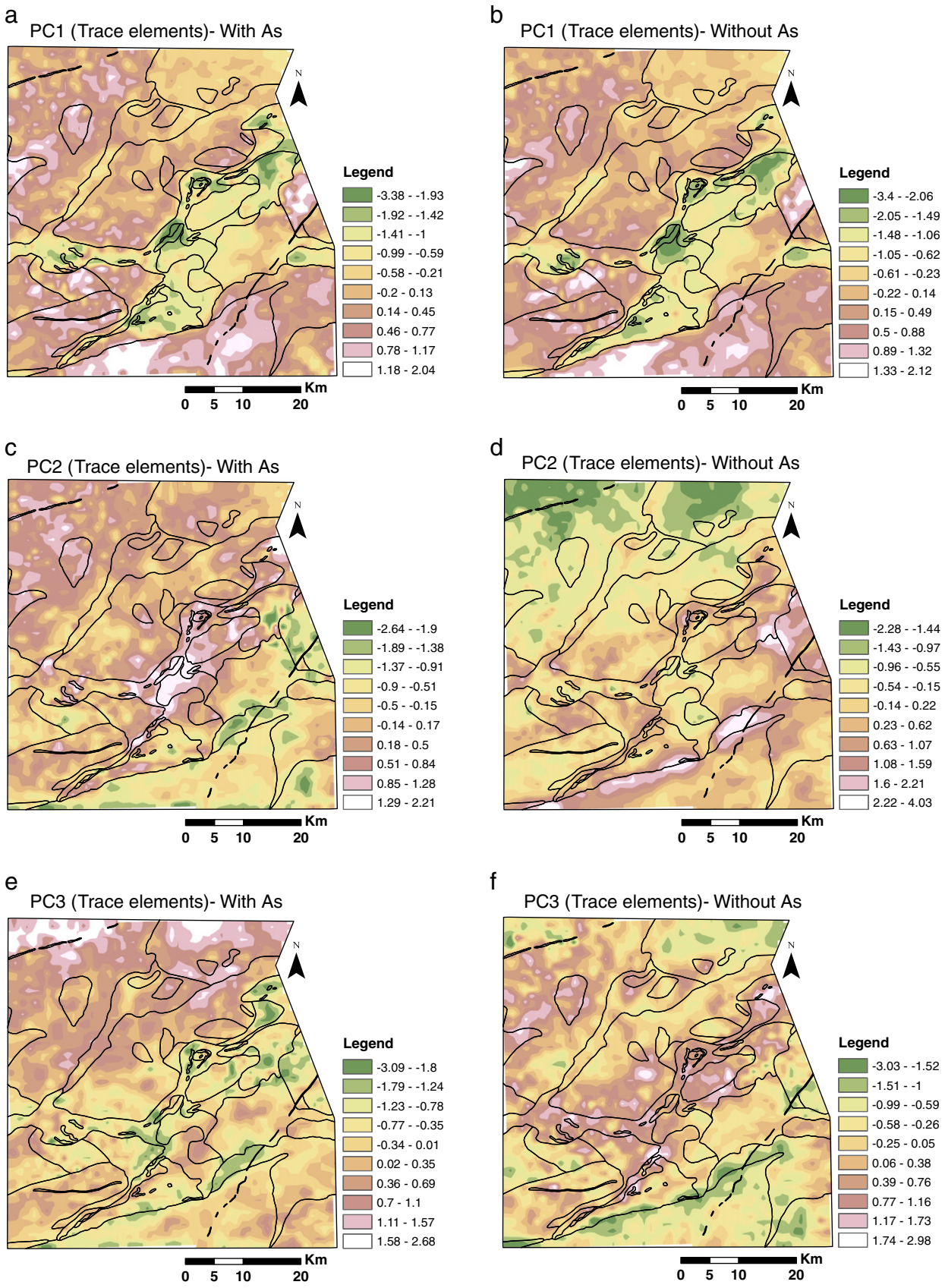

Fig. 4. Interpolated images of PCs of the clr-transformed data including As with As^r (left panel) and clr-transformed data excluding As (right panel) of (a) PC1 scores of clr-transformed data; (b) PC2 scores of clr-transformed data; (c) PC3 scores of clr-transformed data. All maps were interpolated using the inverse distance weighting (IDW) method and a cell size of 1 * 1 km. Thin black lines represent lithological contacts, and for the legend see Fig. 2.

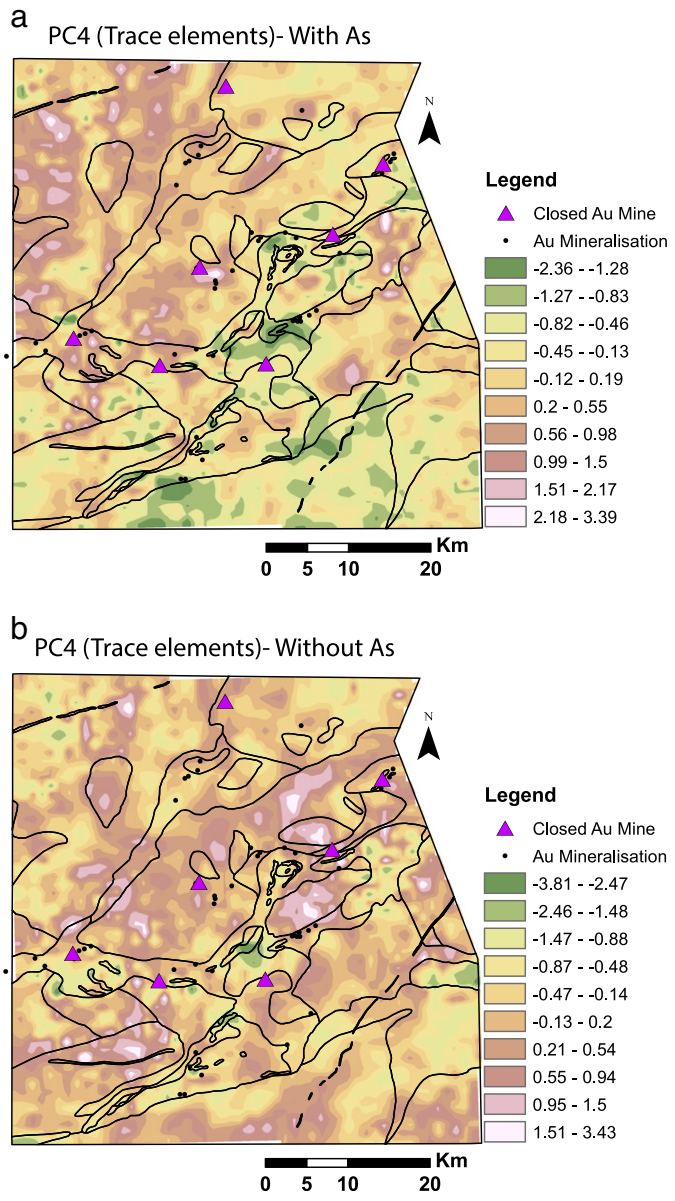

Fig. 5. Interpolated images of (a) PC4 scores of clr-transformed data including censored As with As^r representing Sb–As–Te–Cr–Au association reflecting the gold mineralisation; (b) PC4 scores of clr-transformed data excluding As values representing weathering, concentration of heavy minerals and GGB. All maps were interpolated using the IDW method and a cell size 1 * 1 km. Thin black lines represent lithological contacts, and for the legend see Fig. 2.

of study area shows positive log (Sr/Rb) ratios, whereas granodiorite in the south-eastern part of the area exhibits negative log (Sr/Rb) ratios. The log (Ga/V) ratio discriminates the mafic–ultramafic-dominated greenstone belt from the granitic terrain. The former unit is characterised by positive values of log (Ga/V) ratios, while the latter displays negative values of log (Ga/V) ratios. Within the greenstone belt, the ultramafic rocks exhibit slightly more negative values of log (Ga/V) ratios compared to the mafic rocks (Fig. 7b). The log (Cr/Zr) ratio depicts variations in various rock types with positive, near zero and negative values reflecting ultramafic, mafic and granitic rocks, respectively (Fig. 7c).

Log-ratio maps were also plotted using the major element data. The log (K_2O/Fe_2O_3) map (Fig. 8a) reflects K-rich rocks (granitoids) versus mafic and ultramafic units, with the ultramafic units within GGB clearly showing negative values of log (K_2O/Fe_2O_3). Positive values of log (Na_2O/CaO) ratios are characteristic of the granitic terrain, whereas negative values of log (Na_2O/CaO) ratios characterise the greenstone belt (Fig. 8b). The log (MgO/Al_2O_3) ratio map (Fig. 8c) discriminates between the ultramafic–mafic–granite and the gneiss. Positive values of log (MgO/Al_2O_3) ratios clearly outline the ultramafic units, and values of near zero to weak negative ratios outline mafic-dominated areas, while strong negative values of log (MgO/Al_2O_3) ratios indicate granitoid rocks.

Combining single element or element ratio maps into colour composite maps is also useful for extracting or visualising geochemical information related to lithology. Fig. 9a displays a composite map of major oxide log-ratios, which aid in discriminating between, particularly, ultramafic–mafic–granite–gneiss in the entire study area. Fig. 9b is a colour composite map of the log-ratio maps of trace element data. This map best discriminates the various rock units, including ultramafic rocks–iron formation (dark blue), mafic rocks (violet) and younger granitoids with no migmatisation (yellow-orange) and older granitoids with migmatisation (green). A discernible variation within the granitoids is also clearly displayed on this map.

5. Discussion

In exploration or applied geochemistry, the main aim of PC analysis is reduction of dimensionality of data to find the first few principal components, expressing as much of the inherent variability of the complete data set as possible. The statistical analysis of compositional multivariate data is much discussed by statisticians and geochemists. The log-ratio transformation methodology represents a powerful set of methods and techniques for statistical analysis of compositional data (Martin-Fernández et al., 2012). There is lack of research and documentation on compositional data analysis versus theoretical research (Carranza, 2011). In this study, PC analysis of ln- and clr-transformed data was performed by including and excluding As data with censored values substituted by ½ DL.

Clr-transformation in this study revealed multi-element associations in PCs of trace element data that are valuable for mapping and exploration. The clr-transformation yielded trace-element associations that can be related to the present known lithology and gold mineralisation in the GGB (e.g., association of As–Te–Sb–Cr representing gold mineralisation in the GGB). The clr-transformation, compared to ln-transformation, enhances multi-element associations due to lithology or weathering processes and particularly the 4th PC revealed an association of elements related to the gold mineralisation in the GGB.

The results show that PC analysis is able to discriminate the major lithologies (mafic, ultramafic, mafic–ultramafic, old and younger granitoids) fairly well, thereby resulting in the improvement of the existing lithological map. The results were validated using some detailed lithological maps in the gold-mineralised areas (e.g., Billay et al., 2009; Pretorius et al., 1988; Prinsloo, 1977). As field observations indicate that most of the gold occurrences are hosted in mafic–ultramafic rocks, and as most of the known gold occurrences occur in the areas interpreted from this study to be underlain by mafic and mafic–ultramafic assemblages of the greenstone belt, the interpretive bedrock map will be useful in improving the accuracy of identifying favourable areas for gold prospecting.

The results of analysis of soil data in the GGB imply that the soil data can be used to aid bedrock mapping, as revealed by chemical variations in the various types of granitic gneiss, reflecting either variation in the degree of migmatisation, and/or multiple phases of intrusion. The north-eastern part of the study area, which was previously mapped as granitic gneiss, is in conflict with respect to results of the geochemical data analysis. Whereas the log-ratio maps, log (Ga/Va), log (Cr/Zr), log (Na_2O/CaO) and the composite map of PCs of trace element data show patterns similar to the rest of the granite gneiss (Goudplaats gneiss); the log (Sr/Rb) map and the composite map of major oxide data PCs display different signatures compared to gneiss in the rest of the study area. The log (K_2O/Fe_2O_3) ratio map depicts signatures similar to the mafic–ultramafic assemblages. Carranza et al. (2013) observed that

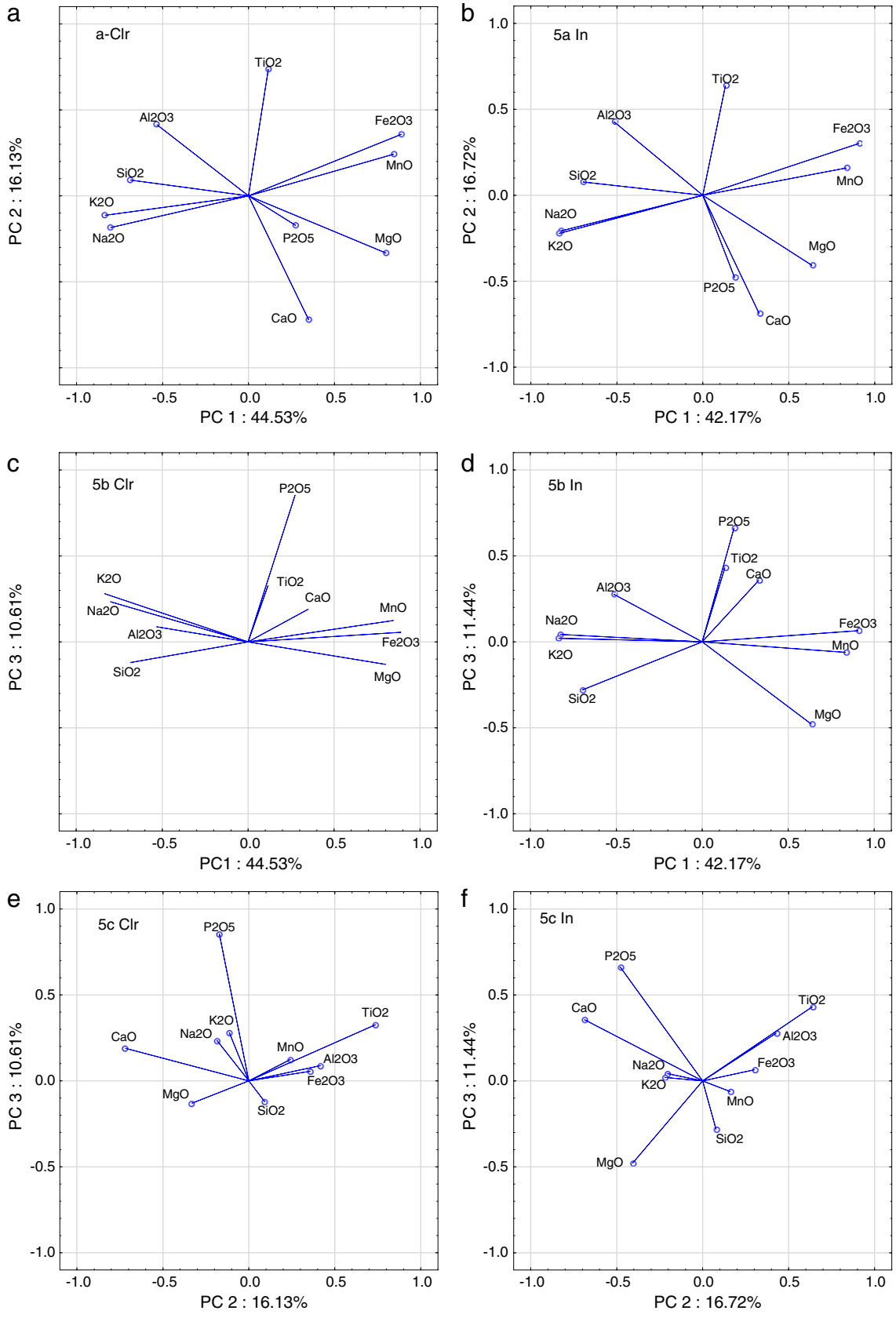

Fig. 6. Major oxide biplots of PCs of the clr-transformed (left panel) and ln-transformed (right panel) major oxide data: (a) PC1 vs. PC2; (b) PC1 vs. PC3; (c) PC2 vs. PC3.

the airborne radiometric data signature of this area is similar to the main greenstone belt. This, somewhat, conflicting results suggest that the north-eastern part of the study area is underlain by a mixture of rock types (granitic gneiss and mafic–ultramafic rocks). Interpretation of gravity maps (Bouger anomaly, Airy-Heiskanen isostatic anomaly, residual gravity anomaly) by Kleywegt et al. (1987), suggest that the

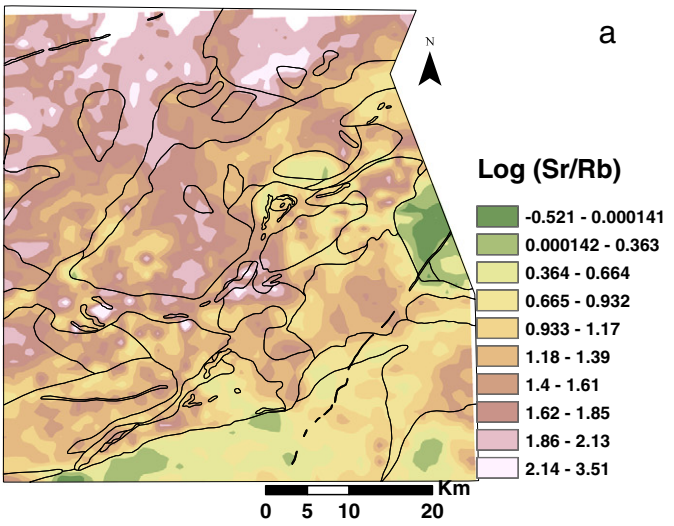

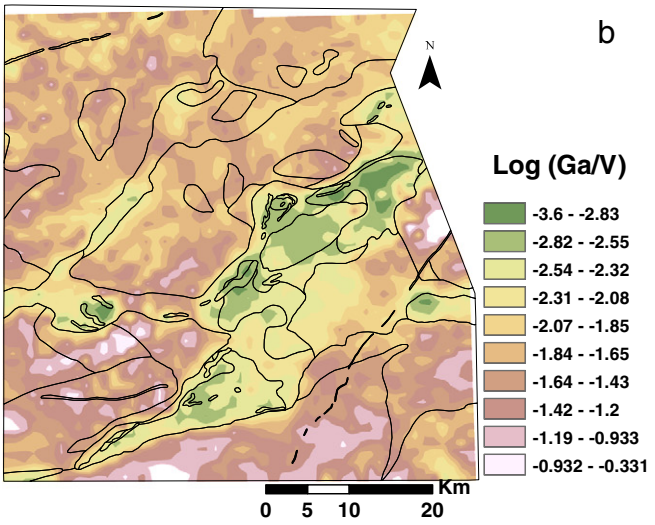

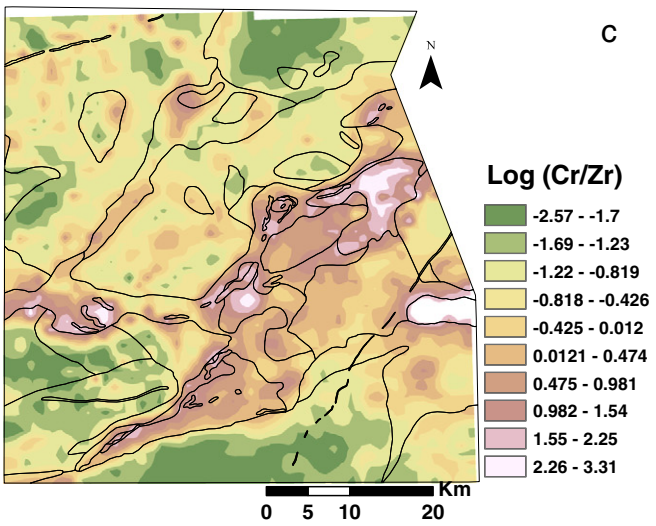

Fig. 7. Maps of element ratios (log-transformed) showing the various bedrock units: (a) Sr/Rb; (b) Ga/Va and (c) Cr/Zr. All maps were interpolated using the IDW method and a cell size of 1 * 1 km. Thin black lines represent lithological contacts, and for the legend see Fig. 2.

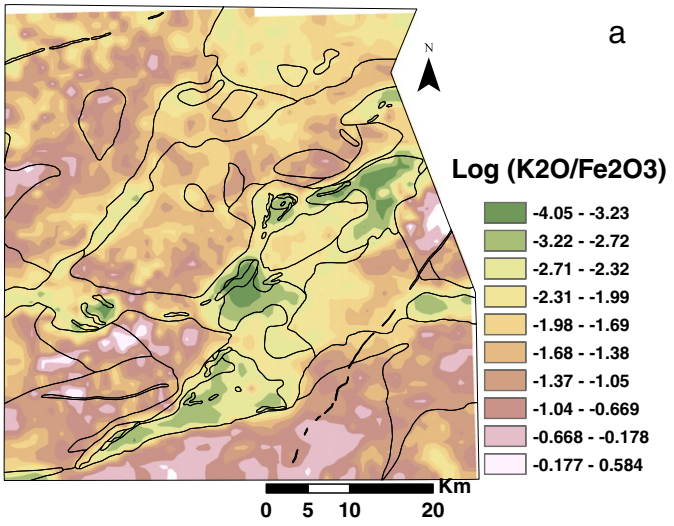

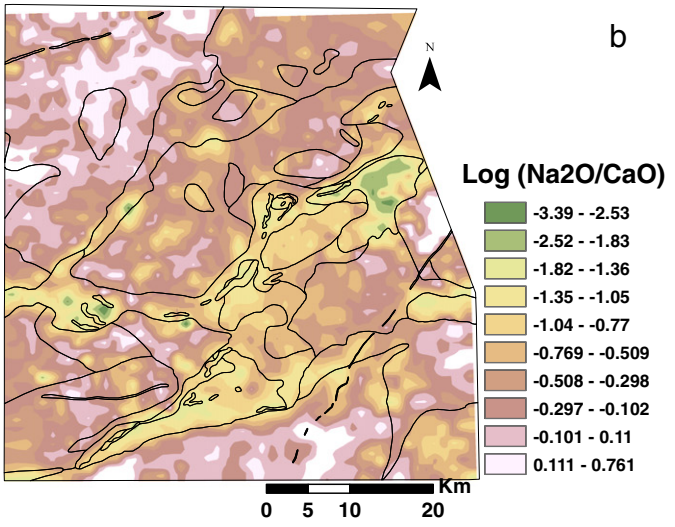

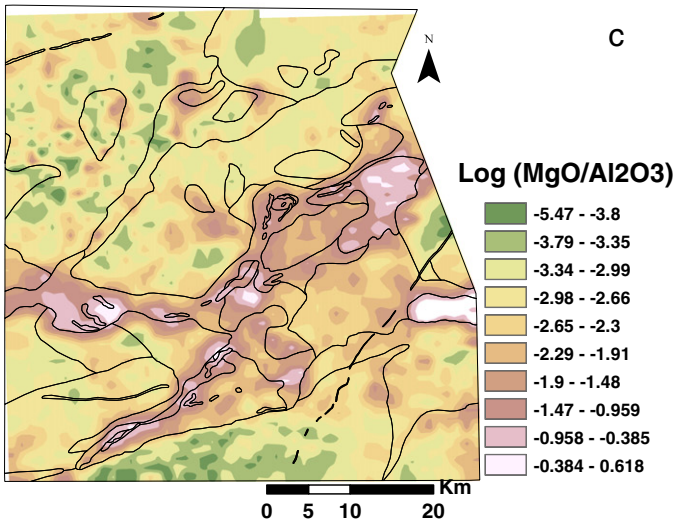

Fig. 8. Maps of major oxide ratios (log-transformed) representing differences in lithology: (a) (K_2O/Fe_2O_3); (b) (Na_2O/CaO) and (c) (MgO/Al_2O_3). All maps were interpolated using the IDW method and a cell size of 1 * 1 km. Thin black lines represent lithological contacts, and for the legend see Fig. 2.

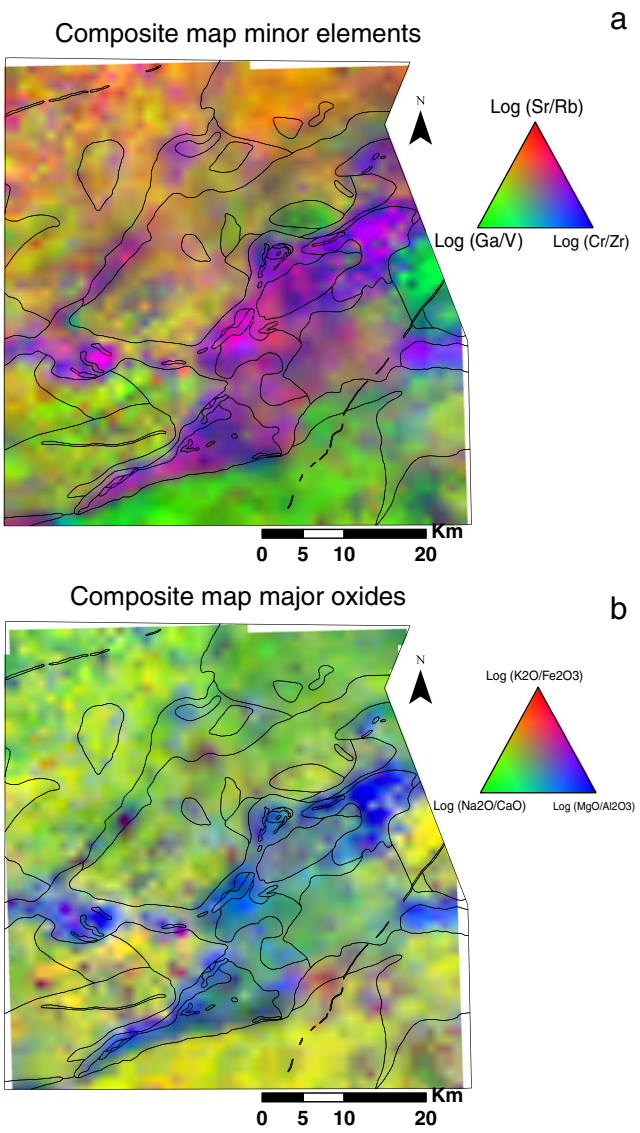

Fig. 9. Colour composite images: (a) trace element ratios (log-transformed), R = (Sr/Rb), G = (Ga/V), B = (Cr/Zr); (b) major oxides ratios (log-transformed), R = (K_2O/Na_2O), G = (Na_2O/CaO), B = (MgO/Al_2O_3). Thin black lines represent lithological contacts, and for the legend see Fig. 2.

north-eastern part of the study area is underlain by gneiss. As the log (K_2O/Fe_2O_3) ratio map and radiometric data indicate the presence of mafic–ultramafic rocks, the north-eastern part of the study area is interpreted to be dominantly underlain by granitic gneiss with minor intercalations (rafts) of mafic–ultramafic rocks. The Manvil gold prospect (Fig. 2) is a good example of a known greenstone remnant within gneiss. Widespread remnants of Archaean greenstone belts in the Kaapvaal Craton have also been described by Brandl et al. (2006). The presence of small zones of mafic–ultramafic rocks in this area suggests that a higher density soil sampling programme has the potential to outline mafic–ultramafic rocks that may have a potential for gold mineralisation.

Previous studies (Alchin and Visser, 1986; Billay et al., 2009; Ehlers, 1985b) have identified arsenic as a pathfinder for gold mineralisation in the GGB. Arsenopyrite mineralisation or As enrichment in soil has been described in relatively well investigated gold deposits in the GGB (McCourt and Legodi, 1983; Pretorius et al., 1988; Weilers, 1956). Billay et al. (2009) found As to be a useful pathfinder for gold mineralisation in the GGB, based on existing litho-geochemical and soil data on some of the deposits. This is corroborated by high loadings of As and Sb (there is no previous data of Sb) on PC4 (Table 1), which reflect the presence of gold mineralisation. Background levels of As have been observed, however, in the upper soil horizon over gold mineralised areas, but concentrations of As distinctly increase with depth (Alchin and Visser, 1986; Ehlers, 1985a). This suggests that soil samples should be collected from deeper horizons during follow-up soil sampling campaigns in prospective areas identified in this study.

6. Conclusions

Based on the results presented above, the following conclusions can be made:

(1) Soil geochemical data can be used to characterise, interpret and map bedrock under regolith cover in the Giyani greenstone belt.
(2) The application of multivariate analysis, particularly principal component analysis, is able to highlight the major bedrock units in the Giyani area, and to discriminate between mafic and ultramafic assemblages within the area.
(3) The first three principal components of either trace element or major oxide data sets, and the composite maps of the PC maps show significant contrast between mafic, ultramafic and granitoid rocks and various types of granitoids in the study area.
(4) The trace element data yield a principal component (PC4) representing an association of pathfinder elements, and outline prospective areas of gold mineralisation in the GGB.
(5) Log-ratio maps of major oxide and trace element soil data are useful for bedrock mapping. Colour composite images of PCs of either major oxide or trace element data in soil are useful for evaluating the underlying bedrock in areas with scarce outcrop.
(6) Centred log-ratio (clr) transformed soil geochemical data provide enhancement of multivariate association patterns reflecting the presence of gold mineralisation in the GGB, as compared to ln-transformed soil geochemical data; a conclusion similar to other real documentation and research on compositional data approach.
(7) Inclusion of about 40% of samples with censored values for As (replaced by ½ of detection limit) results in anomalous multi-element associations that are similar to those obtained by exclusion of the As data. Thus, inclusion of about 40% of samples with censored values for a pathfinder element (e.g., As) does not affect interpretation and mapping of multi-element anomalies reflecting the presence of mineralisation.

Acknowledgement

This study was funded by a joint venture between the CGS and the Meeting Points mining project of the Swedish Geological Survey (44033). Thanks to George Morris for his valuable comments and edit on this paper. The reviewers, Vera Pawlowsky-Glahn and Alecos Demetriades, are thanked for their valuable and constructive comments and suggestions, which greatly improved the presentation of material in the paper.

References

Aitchison, J., 1986. The statistical analysis of compositional data. Monographs on Statistics and Applied Probability. Chapman & Hall Ltd., London (UK) (416 pp.).
Alchin, D.J., Visser, D., 1986. Exploration for Gold in the Northern Contact Zone of the Giyani Greenschist Belt, Giyani Group, Gazankulu. Unpublished Report no.STK-2343, Council for Geoscience, Pretoria.
Armstrong, R.C., Compston, W., De Wit, M.J., Williams, I.S., 1990. The stratigraphy of the 3.5–3.2 Ga Barberton greenstone belt revisited: a single zircon ion microprobe study. Earth Planet. Sci. Lett. 101, 90–106.
Barnes, S.J., 1990. The use of metal ratios in prospecting for platinum-group element deposits in mafic and ultramafic intrusions. J. Geochem. Explor. 37, 91–99.
Barton, J.M., Van Reenen, D.D., 1990. Constraints on the timing of the Limpopo Orogeny. In: Barton, J.M. (Ed.), The Limpopo Belt: A Field Workshop on Granulites and Deep Crustal

Tectonics. Extended Abstracts Volume. Rand Afrikaans University, Johannesburg and Foundation for Research and Development, Pretoria, pp. 10–12.
Beus, A.A., Grigorian, S.V., 1977. Geochemical Exploration Methods for Mineral Deposits. Applied Publishing Ltd., Wilmette, Illinois, U.S.A. (287 pp.).
Billay, A.Y., Ngcofe, L., Matshivha, M., 2009. GIS-based Gold Prospectivity Mapping of the Giyani Greenstone Belt. Unpublished Report No 2009-0010, Council for Geoscience, Pretoria.
Billay, A.Y., Sadeghi, M., Carranza, E.J.M., 2014. Predictive Mineral Prospectivity and Bedrock Mapping in the Giyani Greenstone Belt, South Africa. Unpublished Report no STK-2014-0027. Council for Geoscience, Pretoria.
Bonham-Carter, G.F., Agterberg, F.P., Wright, D.F., 1988. Integration of geological datasets for gold exploration in Nova Scotia. Photogramm. Eng. Remote Sens. 54 (11), 1585–1592.
Bonham-Carter, G.F., Agterberg, F.P., Wright, D.F., 1989. Weights of evidence modeling: a new approach to mapping mineral potential. In: Agterberg, F.P., Bonham-Carter, G.F. (Eds.), Statistical Applications in the Earth Sciences. Geological Survey of Canada 98, pp. 171–183.
Brand, N.W., 1999. Element ratios in nickel sulphide exploration: vectoring towards ore environments. J. Geochem. Explor. 67, 145–165.
Brandl, G., Cloete, M., Anhaeuser, C.R., 2006. Archean greenstone belts. In: Johnson, M.R., Anhaeuser, C.R., Thomas, R.J. (Eds.), The Geology of South Africa. Geological Society of South Africa, Johannesburg/Council for Geoscience, Pretoria, pp. 9–56.
Carranza, E.J.M., 2009. Geochemical anomaly and mineral prospectivity mapping in GIS. Handbook of Exploration and Environmental Geochemistry vol. 2 (352 pp.).
Carranza, E.J.M., 2010. Mapping of anomalies in continuous and discrete fields of stream sediment geochemical landscapes. Geochem. Explor. Environ. Anal. 10, 171–187.
Carranza, E.J.M., 2011. Analysis and mapping of geochemical anomalies using logratio-transformed stream sediment data with censored values. J. Geochem. Explor. 110, 167–185.
Carranza, E.J.M., Sadeghi, M., Billay, A., 2013. Data integration for interpretive bedrock mapping in the Giyani area (South Africa). 12th SGA Biennial Meeting 2013-Proceedings vol. 2, pp. 472–476.
Chao, T.T., Theobald, P.K., 1976. The significance of secondary iron and manganese oxides in geochemical exploration. Econ. Geol. 71, 1560–1569.
Cheng, Q., Xu, Y., Grunsky, E., 2000. Integrated spatial and spectrum method for geochemical anomaly separation. Nat. Resour. Res. 9, 43–52.
Cicchella, D., De Vivo, B., Lima, A., Albanese, S., Fedele, L., 2008. Urban geochemical mapping in the Campania region (Italy). Geochem. Explor. Environ. Anal. 8 (1), 19–29.
Davis, J.C., 1973. Statistics and Data Analysis in Geology. J. Wiley & Sons, Inc., N.Y. (550 pp.).
Davis, J.C., 1986. Statistics and Data Analysis in Geology. John Wiley & Sons. Inc., N.Y. (646 pp.).
Davis, J.C., 2002. Statistics and Data Analysis in Geology. John Wiley and Sons, Inc., p. 2002 (638 pp.).
De Quadros, T.F.P., Koppe, J.C., Strieder, A.J., Costa, J.F.C.L., 2003. Gamma-ray data processing and integration for lode-Au deposits exploration. Nat. Resour. Res. 12, 57–65.
De Wit, M.J., Van Reenen, D., Roering, C., 1992. Geologic observations across a tectono-metamorphic boundary in the Babangu area, Giyani (Sutherland) greenstone belt, South Africa. Precambrian Res. 55, 111–122.
Egozcue, J.J., Pawlowsky-Glahn, V., Mateu-Figueras, G., Barcelo-Vidal, C., 2003. Isometric logratio transformation for compositional data analysis. Math. Geol. 35, 279–300.
Ehlers, D.L., 1985a. The Mercury Arsenic and Base Metal Trace Element Signatures in Soils Above Fourteen Known Gold Deposits in the Giyani Group, North-Eastern Transvaal. Unpubl Report no. STK-2192, Council for Geoscience, Pretoria.
Ehlers, D.L., 1985b. Ka-Mapayeni arsenic anomaly Gazangulu. Unpublished Report No. STK-2552, Council for Geoscience, Pretoria.
El-Makky, A.M., 2011. Statistical analyses of La, Ce, Nd, Y, Nb, Ti, P, and Zr in bedrocks and their significance in geochemical exploration at the Um Garayat gold mine Area, Eastern Desert, Egypt. Nat. Resour. Res. 20, 157–176.
El-Makky, A.M., Sediek, K.N., 2012. Stream sediments geochemical exploration in the northwestern part of Wadi Allaqi Area, South Eastern Desert, Egypt. Nat. Resour. Res. 21, 95–115.
Filzmoser, P., 2005. Identification of multivariate outliers: a performance study. Austrian J. Stat. 34 (2), 127–138.
Garrett, R.G., Thorleifoson, L.H., Matile, G., Adcock, S.W., 2008. Till geochemistry, mineralogy and lithology, and soil geochemistry—data from the 1991–1992 Prairie kimberlite study. Geological Survey of Canada (open file 5582, 1CD-ROM).
Grunsky, E.C., 2010. The interpretation of geochemical survey data. Geochem. Explor. Environ. Anal. 10, 27–74.
Grunsky, E.C., Mueller, U.A., Corrigan, D., 2014. A study of the lake sediment geochemistry of the Melville Peninsula using multivariate methods: applications for predictive geological mapping. J. Geochem. Explor. 141, 15–41.
Kleywegt, R.J., De Beer, J.H., Settler, E.H., Brand, G., Duvenhagen, W.A., Day, R.W., 1987. The structure of the Giyani greenstone belt, as derived from geophysical studies. S. Afr. J. Geol. 90, 282–295.
Kürzl, H., 1988. Exploratory data analysis: recent advances for the interpretation of geochemical data. J. Geochem. Explor. 30 (3), 309–322.
Lepeltier, C., 1969. A simplified statistical treatment of geochemical data by graphical representation. Econ. Geol. 64 (5), 538–550.
Lombard, M., De Bruin, D., Elsenbroek, J.H., 1999. High-density regional geochemical mapping of soils and stream sediments in South Africa. J. Geochem. Explor. 66, 145–149.
Luz, F., Mateus, A., Matos, J.X., Gonçalves, M.A., 2014. Cu- and Zn-soil anomalies in the NE border of the South Portuguese zone (Iberian Variscides, Portugal) identified by multifractal and geostatistical analyses. Nat. Resour. Res. 23, 195–215.
Maritz, H., Cloete, H.C.C., Elsenbroek, H., 2010. Analysis of high density regional geochemical soil samples at the council for geosciences (South Africa): the importance of quality control measures. Geostand. Geoanal. Res. 34, 265–273.
Markandeyulu, A., Chaturvedi, A.K., Raju, B.V.S.N., Parihar, P.S., Miller, R., Gooch, G., 2013. Application of high resolution airborne geophysical data in geological modelling of Mohar Cauldron Complex, Bundelkhand Massif, central India: implications for uranium exploration. Explor. Geophys. http://dx.doi.org/10.1071/EG12053.
Martin-Fernández, J.A., Hron, K., Templ, M., Filzmoser, P., Palarea-Albaladejo, J., 2012. Model-based replacement of zeros in compositional data: classical and robust approaches. Comput. Stat. Data Anal. 56, 2688–2704.
McCourt, S., Legodi, J.L., 1983. An Investigation of Possible Zinc Mineralization in the Khavagari Hills West of Giyani, Gazankulu. Unpublished Report, Council for Geoscience, Pretoria.
McCourt, S., Van Reenen, D.D., 1992. Structural geology and tectonic setting of the Sutherland greenstone belt, Kaapvaal craton, South Africa. Precambrian Res. 55, 93–110.
Pawlowsky-Glahn, V., Buccianti, A., 2011. Compositional Data Analysis: Theory and Applications. Wiley (400 pp.).
Pawlowsky-Glahn, V., Egozcue, J.J., Lovell, D., 2013. The product space T (tools for compositional data with a total). In: Hron, K., Filzmoser, P., Templ, M. (Eds.), Proceedings of the 5th International Workshop on Compositional Data Analysis. Technical University of Vienna, pp. 143–152 (http://www.statistik.tuwien.ac.at/CoDaWork/CoDaWork2013Proceedings.pdf).
Pretorius, A.I., Van Reenen, D.D., Barton, J.M., 1988. BIF-hosted gold mineralization at the Fumani mine, Sutherland greenstone belt, South Africa. S. Afr. J. Geol. 91, 429–438.
Prinsloo, M.C., 1977. Die geologie van 'N Gebied in die Omgeving van Giyani, Noorddoos-Transvaal met verwysing na moonttlike economiese mineraalafsetting. Unpublished Thesis, Rand Afrikaan University, Johannesburg.
Reimann, C., Filzmoser, P., Garrett, R.G., Dutter, R., 2008. Statistical Data Analysis Explained. Applied Environmental Statistics with R. Wiley, Chichester, UK (343 pp.).
Reimann, C., Filzmoser, P., Fabian, K., Hron, K., Birke, M., Demetriades, A., Dinelli, E., Ladenberger, A., The GEMAS Project Team, 2012. The concept of compositional data analysis in practice — total major element concentrations in agricultural and grazing land soils of Europe. Sci. Total Environ. 426, 196–210.
Reimann, C., Birke, M., Demetriades, A., Filzmoser, P., O'Connor, P. (Eds.), 2014. Chemistry of Europe's Agricultural Soils — Part A: Methodology and Interpretation of the GEMAS Data Set. Geologisches Jahrbuch (Reihe B 102). Schweizerbarth, Hannover (528 pp.).
SACS (South African Committee for Stratigraphy), 1980. Stratigraphy of South Africa. Part 1 (Comp. Kent L.E.). Lithostratigraphy of the Republic of South Africa, South West Africa/Namibia, and the Republic of Bophuthatswana, Transkei and Venda. Handbook, Geological Survey of South Africa vol. 8 (690 pp.).
Sadeghi, M., Morris, G.A., Carranza, E.J.M., Ladenberger, A., Andersson, M., 2013a. Rare earth element distribution and mineralization in Sweden: an application of principal component analysis to FOREGS soil geochemistry, in: Foley, N., De Vivo, B., Salminen, R. (Guest Eds.), Rare Earth Elements: The Role of Geology, Exploration, and Analytical Geochemistry in Ensuring Diverse Sources of Supply and a Globally Sustainable Resource. Special Issue, J. Geochem. Explor. 133, 160–175.
Sadeghi, M., Petrosino, P., Ladenberger, A., Albanese, S., Andersson, M., Morris, G., Lima, A., De Vivo, B., The GEMAS Project Team, 2013b. Ce, La and Y concentrations in agricultural and grazing-land soils of Europe, in: Foley, N., De Vivo, B., Salminen, R. (Guest Eds.), Rare Earth Elements: The Role of Geology, Exploration, and Analytical Geochemistry in Ensuring Diverse Sources of Supply and a Globally Sustainable Resource. Special Issue, Journal of Geochemical Exploration 133, 202–213.
Sinclair, A.J., 1976. Applications of Probability Graphs. Association of Exploration Geochemists, Nepean, Ontario (95 pp.).
Sinclair, A.J., 1983. Univariate analysis. In: Howarth, R.J. (Ed.), Statistics and Data Analysis in Geochemical Prospecting. In: Govett, G.J.S. (Ed.), Handbook of Exploration Geochemistry vol. 2. Elsevier, Amsterdam, pp. 59–81 (Chapter 3).
Sinclair, A.J., 1986. Statistical interpretation of soil geochemical data. In: Fletcher, W.K., Hoffman, S.J., Mehrtens, M.B., Sinclair, A.J., Thompson, I. (Eds.), Exploration Geochemistry: Design and Interpretation of Soil Surveys. In: Robertson, J.M. (Ed.), Reviews in Economic Geology vol. 3. Society of Economic Geologists, Chelsea, MI, USA, pp. 97–115.
Sinclair, A.J., 1991. A fundamental approach to threshold estimation in exploration geochemistry: probability plots revisited. J. Geochem. Explor. 41, 1–22.
Singer, D.A., Kouda, R., 2001. Some simple guides to finding useful information in exploration geochemical data. Nat. Resour. Res. 10, 137–147.
Stanley, C.R., Noble, R.R.P., 2008. Quantitative assessment of the success of geochemical exploration techniques using minimum probability methods. Geochem. Explor. Environ. Anal. 8 (2), 115–127.
Tennant, C.B., White, M.L., 1959. Study of the distribution of some geochemical data. Econ. Geol. 54, 1281–1290.
Thompson, M., 1983. Control procedures in geochemical analysis. In: Howarth, R.J. (Ed.), Statistics and Data Analysis in Geochemical Prospecting. In: Govett, G.J.S. (Ed.), Handbook of Exploration Geochemistry vol. 2. Elsevier, Amsterdam, pp. 39–58 (Chapter 2).
Tukey, J.W., 1977. Exploration Data Analysis. Addison-Wesley, Reading (688 pp.).
Ward, J.H.W., Wilson, M.G.C., 1998. Gold outside the Witwatersrand Basin. In: Wilson, M.G.C., Anhaeusser, C.R. (Eds.), The Mineral Resources of South Africa. Handbook. Council for Geoscience vol. 16, pp. 350–386.
Weilers, B.F., 1956. The Geology of the Klein Letaba Gold Mine in the Sutherland Range, Northern Transval. Unpublished M.Sc. Thesis. Stellenbosch University, 33. Series A, Nr 6–11.
Ziaii, M., Carranza, E.J.M., Ziaii, M., 2011. Application of geochemical zonality coefficients in mineral prospectivity mapping. Comput. Geosci. 37, 1935–1945.
Zuo, R., 2011. Identifying geochemical anomalies associated with Cu and Pb–Zn skarn mineralization using principal component analysis and spectrum–area fractal modeling in the Gangdese Belt, Tibet (China). J. Geochem. Explor. 111, 13–22.